Robust Dense Registration of Partial Nonrigid Shapes

Tingbo Hou, *Student Member*, *IEEE*, and Hong Qin, *Senior Member*, *IEEE*

Abstract—This paper presents a complete and robust solution for dense registration of partial nonrigid shapes. Its novel contributions are founded upon the newly proposed heat kernel coordinates (HKCs) that can accurately position points on the shape, and the priority-vicinity search that ensures geometric compatibility during the registration. HKCs index points by computing heat kernels from multiple sources, and their magnitudes serve as priorities of queuing points in registration. We start with shape features as the sources of heat kernels via feature detection and matching. Following the priority order of HKCs, the dense registration is progressively propagated from feature sources to all points. Our method has a superior indexing ability that can produce dense correspondences with fewer flips. The diffusion nature of HKCs, which can be interpreted as a random walk on a manifold, makes our method robust to noise and small holes avoiding surface surgery and repair. Our method searches correspondence only in a small vicinity of registered points, which significantly improves the time performance. Through comprehensive experiments, our new method has demonstrated its technical soundness and robustness by generating highly compatible dense correspondences.

Index Terms—Dense registration, partial nonrigid shape, heat kernel coordinates.

✦

1 INTRODUCTION

DYNAMIC shapes are ubiquitous in various real-world applications. To model unorganized fragments of a dynamic shape in the space-time domain toward model completion and its deformable behavior, it is imperative to establish correct dense correspondences among partial shapes, i.e., to register them accurately. In this paper, we refer registration to a compact matching of two shapes. In recent years, the problem of shape matching has received considerable attention in computer graphics [1], [2], [3], [4], [5], [6], [7], [8], [9]. Here, we address the dense registration of nonrigid partial shapes, with foreseen challenges in the following aspects. First, dynamic shapes are frequently nonrigid, which force us to seek new methods of working with intrinsic "coordinates" rather than extrinsic ones in Euclidean domain. Second, the fragments acquired from the object are partial shapes with overlapping regions and changing boundaries. Therefore, the globally defined coordinates are not applicable, including the shape-DNA [10], the global point signature [11], mean value coordinates [12], and harmonic coordinates [13], to name just a few. Third, the output correspondences must be dense, which is compounded by more difficulties, including accuracy of registration, geometric and topological compatibility, computational efficiency, etc.

To establish a compact matching, dense registration typically needs some intrinsic coordinates to parameterize and index points on the shape. Since we are concentrating on partial shapes of natural nonrigid objects (e.g., faces, articulated objects), the coordinates must be invariant to natural deformation, and they should be determined only by *local* geometry while avoiding negative effects from changing boundaries and topological variation. Heat kernel, as a fundamental solution of the heat diffusion on manifolds, has been applied to indexing points in the heat kernel map (HKM) [6] and the heat triangulation [14]. It measures the heat transferred from one point to another. As time increases, heat spreads out toward a growing neighborhood that elegantly bridges the local and global characteristics in a multiscale sense. This multiscale property gives rise to an intrinsic connection between the diffusion and time. Heat kernel is also relevant to the statistical probability of connecting paths (e.g., random walks in a Brownian motion). Therefore, it is very stable under inelastic deformation, noise, and small topological holes, which is destined as a promising tool for shape registration as well as other problems in computer graphics.

For local coordinates, using anchored references is a popular strategy to position points. For example, the HKM employs one or multiple reference points, and the heat triangulation utilizes d points for d dimensional manifold. For points on the shape, the geometric relations with anchors measured by some metric can be used as their coordinates. With this parameterization, the registration can be conducted by searching correspondences with closest distances of intrinsic coordinates. The searching scheme also plays an important role in registration. A commonly used approach is the nearest-neighbor (N-N) search [3], [6], [15] in the entire searching domain. However, this scheme does not consider geometric compatibilities between correspondences. Here, the geometric compatibility means that points on one shape should have compatible geometric
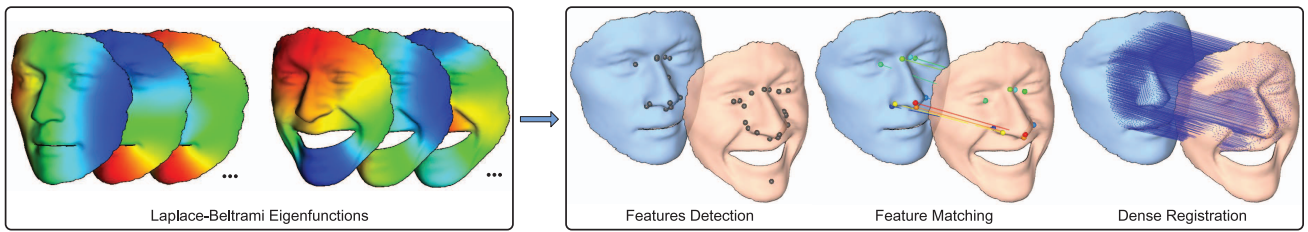
Fig. 1. The architecture of our method highlights a complete solution for shape registration. It computes the Laplace-Beltrami eigenfunctions, by which three steps proceed: feature detection, feature matching, and dense registration.

relations with their corresponding points (if such points indeed exist) on the other shape. In a nutshell, the points are registered compatibly. An improved strategy is to use "voting" [3], [16] from more than sufficient coordinates to decide the optimal location of a correspondence. Although voting can enhance the robustness of positioning by multiple locations in a statistical sense, it does not explicitly ensure the geometric compatibility either.

In this paper, we develop a robust solution for dense registration of partial nonrigid shapes. The central idea of our method is to index all points on the shape by local coordinates and establish dense correspondences via propagation from feature anchors to all other points. As shown in Fig. 1, it proceeds in three main steps: feature detection, feature matching, and dense registration, all of which are hinged upon heat kernels approximated from the Laplace-Beltrami eigenfunctions. We adopt the heat kernel signature (HKS) [17], referring to the heat kernel from one point to itself (i.e., the main diagonal of the heat kernel matrix), to find features on the shape. The detected features are matched using a graph matching method [18] with adaptive multiscale measurements based on heat kernels. We select reference points from the matched features, and conduct registration directly on the shape. Unlike previous parameterization-based methods [3], [16], [19], our method does not need to flatten the surface into a lower dimensional space. It accommodates complex shapes with great flexibility without surface surgery and repair. Moreover, because of the probability property of random walks, our method is robust to noise and small holes. Key contributions in our new method include:

- We articulate the concept of "positioning," referring to the procedure of locating a point on a shape, and employ it to design and match point indices. Good indices should have accurate positioning and toleration to boundary changes.
- We propose the heat kernel coordinates (HKCs), which have a strong positioning ability that can locate and index points accurately. The HKCs are multiscale outputs of heat kernels from multiple sources to points on the surface. In our work, the sources (i.e., reference points) are obtained from feature matching.
- We develop a fast algorithm to propagate correspondence by searching local vicinities of registered points, following the priority order of their HKCs. The proposed algorithm is named "priority-vicinity search," which ensures the geometric compatibility and optimizes the location of correspondence.

- We provide a complete solution for shape registration, which automatically builds dense correspondences between two partial shapes. This solution is robust to noise, and can even handle different but similar shapes.
- We conduct various experiments to demonstrate the performance of our method both visually and quantitatively.

2 PREVIOUS WORK

This section briefly discusses relevant work in three categories: shape feature, shape matching, and shape registration. Here, we categorize the related work as matching or registration, according to whether it is carried out on selected points or compact areas. These two categories usually have different purposes involving different techniques. For an elaborated and comprehensive taxonomy of shape correspondence, we refer readers to a recent survey [9].

Shape feature. Feature extraction plays a critical role in many graphics problems. Specifically, for registration, it provides sufficient points to anchor and stitch different shape pieces, which should be salient, stable, and representative. Shape features can be interpreted as local extrema of some geometric quantities, such as normal [20], curvature [21], [22], and geometry image [23], [24]. Local geometric characteristics are usually sensitive to mesh perturbation and resolution. So multiscale property is much more desirable, and its construction should be stable. Shape features can also be described by global properties, such as Laplace-Beltrami eigenvalues [10] and eigenfunctions [11]. Nevertheless, global properties are easily affected by changes of topology and geometric boundary. Recently, Sun et al. [17] proposed the HKS to describe and detect manifold features. The HKS is an intrinsic property that indicates the diffusion process in different time (scales), naturally bridging local and global information. It starts to gain more popularity in the state-of-the-art for its merits in stableness, multiscale, isometric invariance, and informativeness. It has been successfully applied to shape matching and registration [5], [6]. Vaxman et al. [25] proposed a multiresolution approach to improve the computational efficiency of HKS for large meshes. In [26], convolution based on heat kernels was used to find multiscale features.

Shape matching. Shape matching is to match selected points on shapes, with purposes in shape recognition and retrieval. In graphics, the topic of shape matching starts to gain momentum recently, which is often performed by building a map between two sets of points, or searching common subgraphs of two graphs. Lipman and Funkhouser

[3] utilized conformal mapping and a voting strategy to match samples. In [27], the eigenfunctions of the Laplace-Beltrami operator were employed for shape matching, which are global functions defined on the entire shape. In [6], Ovsjanikov et al. defined the HKM as heat kernels from a fixed reference point, and applied it to shape matching using a simple N-N search. They also extended the one-point method to multiple reference points. In [5], a shape was mapped to a feature space, and represented by feature vectors. The matching of two shapes turns into scoring the shape pair using feature vectors. In [8], a correspondence map was measured by the intersection configuration distance. Bronstein et al. adopted diffusion distance as an isometry-invariant metric in shape recognition [28] and shape matching [29]. In [30], an affine invariant diffusion geometry was proposed for matching deformable shapes, which is invariant to squeeze and shear transformations.

In computer vision, this problem can also be well modeled by the graph matching with pairwise or high-order geometric compatibilities. Leordeanu and Hebert [18] proposed the spectral matching method that constructs a graph by taking each candidate correspondence as a point. Correct correspondences were found by the eigenvector with the largest eigenvalue of the affinity matrix, whose entries are pairwise geometric relations. In [31], Cour et al. improved the second-order graph matching by a spectral relaxation scheme and a normalization procedure. Torresani et al. [32] proposed an optimization technique of high-order graph matching using dual decomposition. Recently, Duchenne et al. [33] extended the spectral matching to the affinity tensor with third-order potentials, which improves the robustness but requires heavy computational load. In [16], a 3D shape was flattened to a 2D image using conformal map in order to adopt the high-order graph matching. However, the surface flattening has strict requirements on topology.

Shape registration. For articulated objects, piecewise rigid transformation [2], [34] was adopted to segment the surface to rigid subparts, lacking of accuracy for nonrigid deformation. For complete nonrigid shapes, global map has been widely used in previous methods. Kraevoy and Sheffer [35] used cross-parameterization to establish a bijective mapping between two surfaces through a common base domain. The mapping from a surface to its base domain is initialized by mean value parameterization, and the triangular interiors in the base domain are registered using barycentric coordinates. Manifold harmonics are also used to register shapes with isometric deformation by spectral embeddings [7], [36], [37], [38], which are limited to shapes with unchanged boundaries. Conformal maps [16], [19] have been applied to register nonrigid surfaces, by flattening a 3D surface to a 2D domain. However, they are usually accompanied by model cutting and hole filling. Therefore, they are very sensitive to topology and boundary changes. In [39], barycentric coordinates of harmonic functions were utilized to establish dense correspondences between shape-from-silhouette surfaces. Multidimensional scaling (MDS) has also been employed to register nonrigid surfaces. Bronstein et al. [40] proposed the generalized MDS to embed 2-manifolds and then match them. Jain and Zhang [1] proposed a shape matching framework by spectral embedding of the geodesic affinity matrices and thin-plate splines. It requires computing geodesics between each pair

of points, and decomposing a dense affinity matrix. For incomplete shapes, Tevs et al. [41] used the RANSAC-like algorithm to match points and refine the registration by the post process based on geodesics. Although it does not enforce strict requirements on topology and boundary of the shape, the geodesics are sensitive to noise and holes.

3 HEAT KERNEL COORDINATES

3.1 Heat Kernel

Let M be a compact Riemannian manifold. The heat diffusion process over M is formulated by the following partial differential equation (PDE), i.e., the heat equation,

$$\frac{\partial u(x,t)}{\partial t} = \Delta u(x,t), \qquad (1)$$

where Δ denotes the Laplace-Beltrami operator on M. The heat kernel $h_t(x,y)$ is known as a fundamental solution of the heat equation, subject to the Dirac condition [42]

$$h_t(x,y) \to \delta_{xy}, \text{ as } t \to 0^+. \qquad (2)$$

The physical meaning is the heat diffused from x to y at time t, with a unit source of heat placed at x.

Assume the Laplace-Beltrami operator Δ has the eigen-decomposition $\{\lambda_k, \phi_k\}_{k=0}^{\infty}$:

$$\Delta \phi_k = \lambda_k \phi_k, \qquad (3)$$

where λ_k and ϕ_k are the kth eigenvalue and corresponding eigenvector of the operator Δ. The spectrum of Δ consists of an increasing positive sequence $\{\lambda_k\}_{k=0}^{\infty}$. The eigenfunctions $\{\phi_k\}_{k=0}^{\infty}$ form an orthonormal basis in L^2, which have been applied to shape segmentation [43], [44], [45]. The heat kernel then has the following eigenfunction expansion formula:

$$h_t(x,y) = \sum_{k=0}^{\infty} e^{-\lambda_k t} \phi_k(x) \phi_k(y). \qquad (4)$$

A numerical solution can be computed by a finite number of eigenfunctions, with discrete Laplace-Beltrami operator [46]. The short-time asymptotic property of the heat kernel is given by [42],

$$\lim_{t \to 0} t \log h_t(x,y) = -\frac{1}{4} d_M^2(x,y), \qquad (5)$$

where $d_M(x,y)$ is the geodesic between x and y on M. For manifolds of bounded geometry (volume) $\mu(M)$, the heat diffusion has a stationary state as:

$$\lim_{t \to \infty} h_t(x,y) = \frac{1}{\mu(M)}. \qquad (6)$$

The heat kernel has many attractive properties, such as isometric invariant, informative, multiscale, and stable, which have been discussed in [17]. In our system, we concentrate on dense registration of partial shapes, so the multiscale nature and the stable property are worthy to be reaffirmed.

The multiscale property states that the heat kernel $h_t(x, \cdot)$ is mainly determined by a neighboring area of x, and the size of the area is related to t. This is because the heat distributed
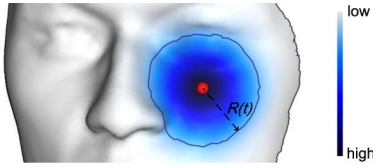
Fig. 2. An upper radius $R(t)$ and its geodesic ball with $t = 20$ and $\epsilon = 0.1$. The color denotes the heat kernels starting from the center.

Fig. 3. Numerical and analytic heat kernels on a triangular mesh of a 2D plane: $h_t(x, x)$ with varying t (left); $h_t(x, y)$ with $t = 10$, and varying distance $|x - y|$ (right).

outside this area is very small, and hence can be ignored. Let $D \subseteq M$ be a compact submanifold of M with smooth boundary, the heat kernel $h_t^D(x, y)$ associated with domain D is a good approximation of $h_t(x, y)$ as long as t is small enough. For more details toward its mathematical proof, we refer readers to [42], [47], [48]. The multiscale property allows us to utilize heat kernel on partial shapes with well-chosen time range that will be discussed in the next section.

The stableness of the heat kernel comes from Brownian motion on manifold, where the heat kernel is interpreted as the transition density function of random walk. A Brownian motion on a manifold is a diffusion with a characteristic operator defined as $1/2\Delta$. The heat kernel $h_t(x, y)$ is equivalent to the probability of a random walk from x to y after time t in the Brownian motion. A concise proof of this equivalence was given in [49]. A random walk is a finite Markov chain that is time reversible. The probability of random walk considers all the connected paths between two points. Therefore, local perturbations of the shape would hardly affect the heat kernel. Particularly, in our system, the partial scans acquired from the scanner may always contain local perturbations such as noise and nonisometric distortion. As a consequence, heat kernel is more stable than other metrics such as geodesic and euclidean distance.

3.2 Time Range

In the usage of heat kernels, how to choose time t is a critical problem that has not been fully explored. According to the multiscale property, a great t corresponds to a large supporting area of the heat kernel. We adopt a time range for heat kernels on partial shapes to ensure appropriate supporting areas.

For a Brownian motion X_t, there is an increasing function $R(t)$ called an "upper radius" [50] if, with probability 1, we have $X_t \in B_{R(t)}(x)$ for all t large enough, where $B_r(x)$ denotes a geodesic ball centered at x with radius r. More precisely, the upper radius gives rise to a theoretic result given in the following theorem.

Theorem 1 (The Law of the Single Logarithm [50]). *Let M be a geodesically complete manifold. Assume that, for some $x \in M$ and all r large enough, the volume*

$$V_r(x) \leq \text{const } r^N,$$

with some $N > 0$. Then for any $\epsilon > 0$, the function

$$R(t) = \sqrt{(N + \epsilon)t \log t},$$

is an upper radius for the process X_t started at any $x \in M$.

Fig. 2 shows an upper radius and its geodesic ball with $t = 20$ and $\epsilon = 0.1$, where the color denotes the heat kernels starting from the center. This theorem provides a practical
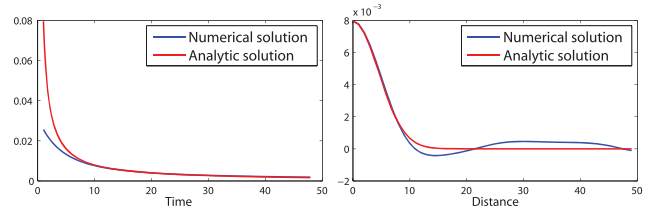
way to obtain an upper radius of a Brownian motion, or equivalently, an upper time $t_u(x)$. We assume that the heat kernel $h_t(x, \cdot)$ with $t < t_u(x)$ can be well approximated by the traversing area of a Brownian motion. Hence, we obtain an upper time $t_u(x)$ for heat kernels starting from x,

$$\sqrt{(2 + \epsilon)t_u(x) \log t_u(x)} = \inf_{y \in \partial M}(d_M(x, y)), \tag{7}$$

with some $\epsilon > 0$. Similarly, we can have a upper time for heat kernels on a closed shape without boundary, by using the longest geodesic as the upper radius.

On the other hand, for discrete surfaces, t also has some lower bound t_l. In our work, we scale the average edge length to be the unit one. Hence, we obtain a lower time $t_l = 1$, which corresponds to one step in a random walk. For small t, the heat kernel $h_t(x, y)$ is close to the Dirac function $\delta_{x,y}$, which indicates the heat kernel $h_t(x, y)$ with $y \neq x$ is very small and therefore error-prone. Moreover, numerical heat kernels are usually computed with finite low-frequency eigenfunctions, which are not adequate for small-scale geometry. Therefore, numerical heat kernels have a lower time $t_l > 1$ depending on the number of eigenfunctions used. We found that for heat kernels computed by $3\% \sim 5\%$ eigenfunctions, $t_l = 4 \sim 8$ would be a reasonable setting. For example, in Fig. 3, we compare the numerical solutions (using 3 percent eigenfunctions) and analytic solutions (i.e., the Gaussian $(4\pi t)^{-1} \exp(-\frac{\|x-y\|^2}{4t})$) on a triangular mesh of a 2D plane. Using our scaling scheme, t is meaningful and equivalent to the one in the analytic solutions. For very small t, the numerical and analytic solutions have large differences, which shows our lower time t_l is in a proper setting. Furthermore, the numerical solutions start to oscillate around the analytic solution when the distance $|x - y|$ is getting larger.

3.3 Heat Kernel Coordinates

In [6], the HKM was defined by the following map

$$\Phi_p^M : M \to F, \quad \Phi_p^M = h_t^M(p, x), \tag{8}$$

where p is a fixed source point, and F is the space of functions from $\mathbb{R}^+$ to $\mathbb{R}^+$. Thus, Φ_p^M associates with every point $x \in M$ a real-valued function of one parameter t given by $h_t^M(p, x)$. The source point p may be any point on manifold M. For a generic connected compact manifold M without boundary and a generic point p on M, the HKM is injective, which indicates $\Phi_p^M(x) = \Phi_p^M(y)$ if and only if $x = y$. This result has been proved by [6].

The HKM has been used for shape matching. However, it has some drawbacks when directly applied to registration
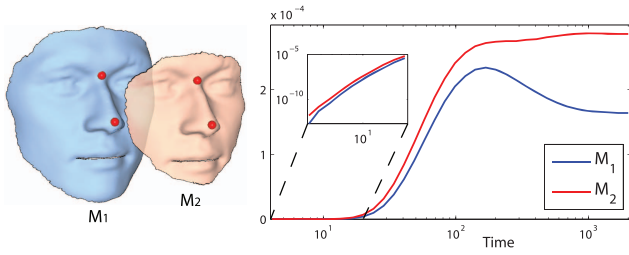
Fig. 4. The time behaviors of two corresponding heat kernels on partial shapes M_1 ($10k$ vertices) and M_2 ($5k$ vertices). In the semilog plot, the heat kernels are close but very small at the beginning, with a log-log plot shown nearby. Then they gradually differ due to boundary changes, and finally converge to different stationary states.

Fig. 5. Position a point x by heat kernels with (a) one-source multitime, and (b) multisource one-time on a plane.

of partial shapes. First, the proof of its injection in [6] relies on $t \to \infty$. For partial shapes, heat kernels are subject to boundary changes at large t. As shown before, t is bounded by a range $[t_l, t_u(x)]$ on partial shapes. Even for complete discrete shapes, numerical heat kernels will converge to a stationary state given by (6), when t is large enough. Fig. 4 shows the time behaviors of two corresponding heat kernels on different partial shapes. At the beginning, the heat kernels are close but very small. Then they gradually differ due to boundary changes, and finally converge to different stationary states. Second, the HKM is not applicable to manifolds whose Laplace-Beltrami operators have repeated eigenvalues [6]. For example, in a plane ($\mathbb{R}^2$), the heat kernel is a Gaussian function. In this case, all the points on a circle centered at p have the same HKM values as shown in Fig. 5a, thus, the HKM is unable to differentiate them. Third, the HKM lacks of sufficient discriminating power in positioning for dense registration. By discriminating power, we mean the ability to distinguish x and y through $\Phi_p^M(x)$ and $\Phi_p^M(y)$. Since the HKM concerns only one heat source, the sense of positioning on partial shapes may be ambiguous, as shown in Fig. 6.

With the time range, we are apt and forced to adopt multiple sources for dense registration. For d-dimensional manifold M, we define the HKCs as a vector of heat kernels produced by the map $\Phi_t : M \to \mathbb{R}^s$ with the number of sources $s > d$:

$$x \to (h_t(x, z_1), \ldots, h_t(x, z_s)), x \in M, \quad (9)$$

where $\{z_1, \ldots, z_s\}$ are source points on M. Multiple sources can offer direction and distance information during indexing, which is analogous to the trilateration technique in navigation and surveying. While this multisource map is an extension of the HKM as mentioned in [6], we provide a complete and robust solution to obtain multiple sources. In fact, we are inspired by the *heat triangulation theorem* for local parameterization in [14].

Theorem 2 (Heat Triangulation Theorem [14]). *Let M be a smooth, d-dimensional compact manifold, and z be a point on M. Let $B_r(z)$ be an embedded ball with center z and radius r. Let $p_1, \ldots, p_d$ be d linearly independent directions. Let y_i be so that $y_i - z$ is in the direction p_i, with $c_4 r \leq d_M(y_i, z) \leq c_5 r$ for each $i = 1, \ldots, d$ and let $t = c_6 r^2$. The map $\Phi : B_{c_1 r}(z) \to \mathbb{R}^d$, defined by*

$$x \to (r^d h_t(x, y_1), \ldots, r^d h_t(x, y_d)),$$

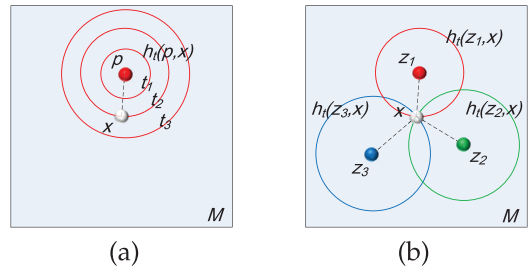*at some t satisfying, for any $x_1, x_2 \in B_{c_1 r}(z)$*

$$\frac{c_2}{r} d_M(x_1, x_2) \leq \|\Phi(x_1) - \Phi(x_2)\| \leq \frac{c_3}{r} d_M(x_1, x_2),$$

with constants $c_1, c_2, c_3, c_4, c_5, c_6 > 0$.

This theorem induces a one-to-one map from a local geodesic ball $B_{c_1 r}(z)$ on the manifold to $\mathbb{R}^d$, which therefore proves the injection of HKCs in this local ball. However, it needs d points with independent directions from center point z, leading to another problem to solve.

Besides some properties inherited from heat kernels, including intrinsic, stable, nonnegative, and multiscale, the HKCs are flexible to conditions of geometry and time. Even for a plane with simple geometry, the HKCs can position a point x as shown in Fig. 5. The HKCs also do not require a large range of time. Fig. 6 shows positioning of different maps: one-source multitime HKM, multisource one-time HKCs, and multisource multitime HKCs, where $t \in [4, 1,024]$ for multitime maps. Within the circles, the color of an arbitrary point y denotes $\|\Phi(x) - \Phi(y)\|_2$, i.e., the discrimination of map Φ at x. The one-source HKM has similar values in a dark ring around the source point, resulting in ambiguities in location for dense registration. Multisource HKCs restrict similar values of $\Phi(x)$ to the dark area close to x, which localizes x with small deviation. Since one-time and multitime HKCs have similar performance of positioning, we will use one-time HKCs in our experiments to reduce computation time and tolerate strict time range. Moreover, we use stable matches of features as source points, resulting in feature-driven HKCs.

4 FEATURE DETECTION AND MATCHING

4.1 Feature Detection

The multiple sources for HKCs require stable matches of salient points between shapes. In our work, we adopt the HKS [17] for feature detection, and the spectral matching [18] for feature matching.
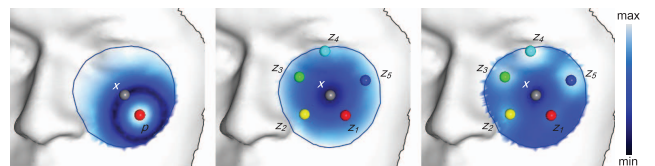

Fig. 6. Positioning of different maps (from Left to Right): one-source multitime HKM, multisource one-time HKCs, and multisource multitime HKCs. Within the circles, the color of a arbitrary point y denotes $\|\Phi(x) - \Phi(y)\|_2$, i.e., the discrimination of map Φ at x.

The HKS is defined as the heat kernel from a point to itself

$$K_t(x) = h_t(x,x). \qquad (10)$$

As a common treatment, we compute it by (4) with a finite number of eigenfunctions. We use the Neumann boundary condition for shapes with boundaries, leading to the fact that the first eigenvalue is always 0. Particularly, we normalize it to balance HKS K_t at different t

$$K_t'(x) = \log\left(\frac{K_t(x)}{(4\pi t)^{-d/2}}\right), \qquad (11)$$

where $(4\pi t)^{-d/2}$ is the HKS in $\mathbb{R}^d$ at time t. For 2-manifolds, the $K_t'(x)$ measures how the surface is curved from a plane with respect to t. HKS features are recognized as local extrema of $K_t'(x)$ at some t. The descriptor of a feature x is a vector of its HKS at a sequence of time t, sampled logarithmically in the range $[t_l, t_u(x)]$. If the feature has $t_u < t_l$, and it is close to the boundary, then we simply eliminate it.

4.2 Feature Matching

We solve the feature matching by a graph matching method from [18], named "spectral matching," but with multiscale measurements based on heat kernels. Assume we have found two feature sets F_1 and F_2 on two shapes. A pair $i = (i_1, i_2)$ denotes a candidate match with i_1 from M_1 and i_2 from M_2. For a candidate pair $i = (i_1, i_2)$, its binary assignment is given by

$$x(i) = \begin{cases} 1, & \text{if } i \text{ is chosen} \\ 0, & \text{otherwise} \end{cases}, \quad \text{with} \quad \sum_{i_1} x(i) \le 1. \qquad (12)$$

The matching problem is equivalent to finding an assignment x that maximizes the objective function with geometric compatibilities.

Let $i = (i_1, i_2)$ be a candidate match in the set

$$F = \{i | (i_1, i_2) \in F_1 \times F_2, d(i) < \epsilon_d\},$$

where $d(i)$ is the distance of two feature descriptors, and ϵ_d is a threshold to determine candidate matches. Specifically, for HKS features, the distance function is defined as

$$d(i) = \left\| K_t'(i_1) - K_t'(i_2) \right\|_2, \text{ with } t \in [t_l, t_u], \qquad (13)$$

where $\| \cdot \|_2$ is the l^2-norm, $t_l = \max(t_l(i_1), t_l(i_2))$, and $t_u = \min(t_u(i_1), t_u(i_2))$. Therefore, this distance has multiple scales *adaptive* to its location. The relations between each pair of candidate matches in F are represented by the affinity matrix A, which is constructed as follows:

1. The entry $A(i,i)$ is the affinity of the correspondence itself, which is computed by

$$A(i,i) = e^{-d(i)^2/2\sigma_1^2}, \qquad (14)$$

where $d(i)$ is defined in (13), and σ_1 is a parameter that is set to be $\sigma_1 = \epsilon_d$ in our work.

2. The affinity $A(i,j)$ represents the geometric compatibility of two candidate correspondences, defined as

$$A(i,j) = e^{-a(i,j)^2/2\sigma_2^2}, \qquad (15)$$

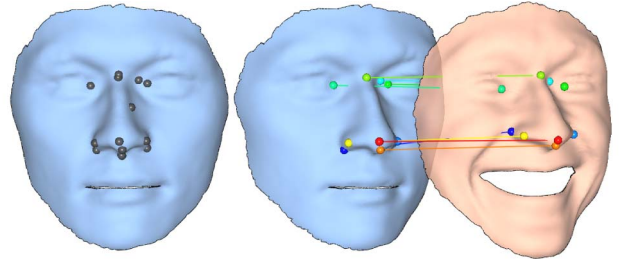where $a(i,j)$ is a function measuring the difference of geometric distances between (i,j):

Fig. 7. Detected features and their matching.

$$a(i,j) = \frac{\|h_t(i_1,j_1) - h_t(i_2,j_2)\|_2}{\|h_t(i_1,j_1)\|_2 + \|h_t(i_2,j_2)\|_2}, \qquad (16)$$

with $t \in [t_l, t_u]$, and the parameter $\sigma_2 = 0.1$.

3. If two candidate correspondences i and j are conflicting (e.g., $i_1 = j_1$ and $i_2 \ne j_2$), we let $A(i,j) = 0$.

The objective function is then represented as

$$J(x) = x^T A x. \qquad (17)$$

Usually, the objective function is relaxed to

$$J'(x) = \frac{x^T A x}{x^T x}. \qquad (18)$$

And the optimal solution maximizes the objective function

$$x^* = \arg\max_x \left(\frac{x^T A x}{x^T x}\right). \qquad (19)$$

It can be solved by computing the leading eigenvector of A. The final assignment is the binary projection of x^*, subject to conflicting constraints. This binary projection algorithm is given in Algorithm 1, where $\epsilon_b = 0.1$ is a threshold to select matches with strong reliabilities. An example of detected features and their matching is shown in Fig. 7, where the color (from red to blue) of matches denotes the selecting order, i.e., the reliability.

Algorithm 1. Binary projection.

Input: optimal solution x^* in Eq. (19)
Output: binary assignment x_b

1 sort x^*;
2 **while** x^* *has element* $> \epsilon_b$ **do**
3   find the greatest element p in x^*;
4      $x_b(p) = 1$;
5   **for** *element* q *in* x^* *that conflicts with* p **do**
6          $x^*(q) = 0$;
7   **end**
8      $x^*(p) = 0$;
9 **end**

---

5 DENSE REGISTRATION VIA HKCS

We find dense correspondences between two shapes by comparing points with their HKCs. An available method in existing work is the nearest-neighbor algorithm, which finds the correspondence of a point as its nearest neighbor in the parametric domain. However, it does not consider the geometric compatibility, by which we mean if two points are close to each other in the reference shape, their
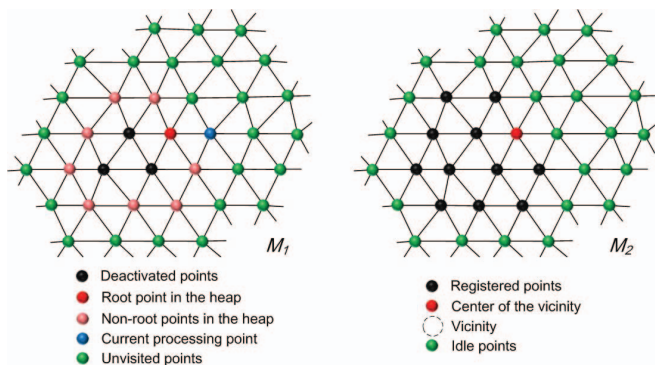
Fig. 8. Illustration of the vicinity search. At this moment, the red point in M_1 is the root of the heap with highest priority. The blue point is a direct neighbor. The algorithm now finds its corresponding point in the blue-shaded vicinity in M_2.

Fig. 9. A reference (blue) shape is registered to a target (pink) shape with $t = 80$. Correspondences in the right figure are color coded, where in the reference shape, the color (changing from red to blue) also denotes the priority.

correspondences in the target shape should also be close. Consequently, there could easily be flips from generated correspondences due to computation error and nonisometric distortion. Furthermore, the global search is time consuming, as a result, the approximated algorithm is often used instead.

To overcome the aforementioned difficulty, our idea is to search correspondences locally in the vicinities of registered points, and propagate correspondence from matched features to other points. That is, for a registered pair (x_1, x_2), a direct neighbor of x_1 only finds its correspondence by their HKCs in the vicinity of x_2. This enforced constraint ensures the geometric compatibility to avoid large flips, but might be trapped into local optima and stop the propagation. Due to the diffusion nature, the positioning of HKCs has different accuracies on the shape. If the registration starts from inaccurately positioned points, it is possible that mismatch will also accumulate during the propagation. Therefore, our novel idea is to define a priority for each point, and initiate the vicinity search by choosing the candidate point with the highest priority. Intuitively speaking, greater heat kernels are more reliable than smaller ones. This naturally motivates us to measure the priority of a point using the magnitude of its HKC, given by

$$P_t(x) = \|(h_t(x, z_1), \ldots, h_t(x, z_s))\|_2. \qquad (20)$$

More precisely, active registered points are inserted into a heap. Each time, the active point with the greatest priority (the root of the heap) is processed, and vicinity searches are initiated for its 1-ring neighbors. Fig. 8 illustrates the procedure of a vicinity search. At this moment, the red point in M_1 is at the root of the heap with the highest priority (key). The blue point is a direct neighbor. The algorithm now finds its corresponding point in the blue-shaded vicinity in M_2. Newly registered points are inserted into the heap, and the current processing point is deactivated. We name the overall algorithm "priority-vicinity search" documented in Algorithm 2, where ϵ_p is a parameter. The computational complexity of this algorithm is $O(N_p N_v \log N_h)$, where N_p is the number of total points, N_v is the vicinity size, and N_h is the size of the heap. In practice, since $N_v \ll N_p$ and $N_h \ll N_p$, the complexity is approximately linear to N. The size of the vicinity, usually set of 2-ring or 3-ring in our experiments, balances the local geometric compatibility and global optimization. That is,
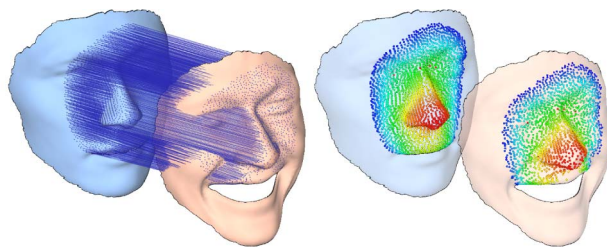
large vicinity size increases the global optimization but decreases the geometric compatibility, and vice versa. We choose to use a small vicinity to ensure the geometric compatibility, since the global optimization may not be stable due to similar or indistinctive patterns in the shape.

Algorithm 2. Priority-vicinity search.

Input: mesh M_1, M_2, source-pair set S
Output: dense correspondences of M_1, M_2

1 heap $H = \emptyset$;
2 **for** *pair* $i = (i_1, i_2)$ *in* S **do**
3   insert i_1 with its priority (key) into H;
4 **end**
5 **while** $H \neq \emptyset$ **do**
6      $x_1 =$ the root of H;
7   delete the root of H;
8   **for** *unregistered direct neighbor* y_1 *of* x_1 **do**
9   **if** *the priority of* $y_1 < \epsilon_p$ **then**
10   continue;
11   **end**
12   find y_2 in the vicinity of x_2, which is closest to y_1 by their HKCs;
13   mark y_1 as registered;
14   output a correspondence (y_1, y_2);
15   insert y_1 with its priority (key) into H;
16   **end**
17 **end**

Fig. 9 shows that a reference (blue) shape is registered to a target (pink) shape with $t = 80$. Correspondences in the right figure are color coded, where in the reference shape, the color (changing from red to blue) also indicates the priority. We will follow this color-coding fashion in our experiments. We adopt matched features as the sources, thus, the registration is both feature driven and feature aligned.

6   EXPERIMENTAL RESULTS

In this section, we first evaluate the proposed method on a benchmark data set [51] with ground truth. Then, we carefully examine our method by conducting comprehensive experiments on various data sets of real scans [51], [52], [53], [54]. A comparison with the multipoint HKM is also conducted. At the end, we show the time performance of our method in the experiments.

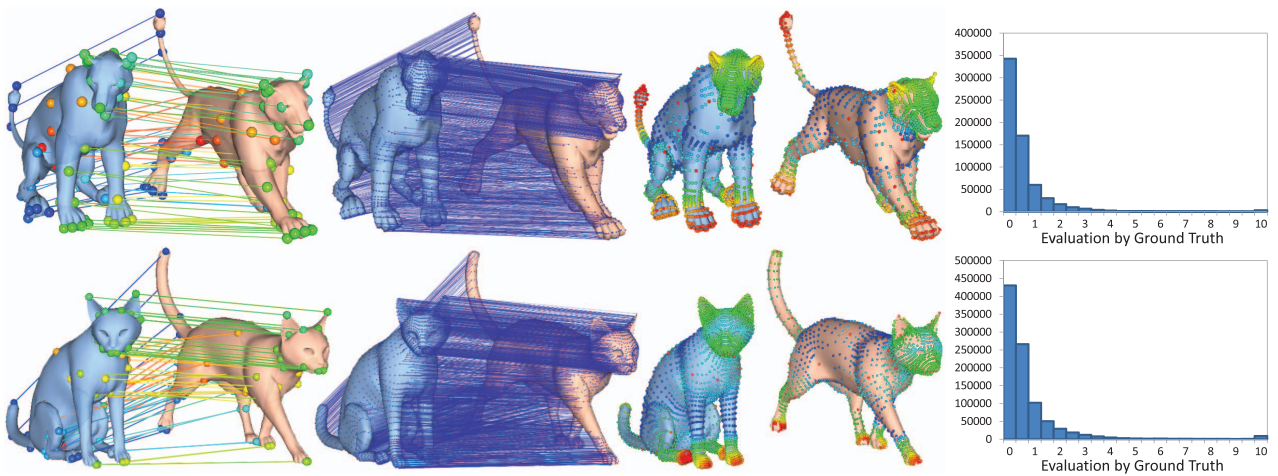**Evaluation on ground-truth data set.** We employ two groups of deformable shapes from the data set, each of

Fig. 10. Evaluation on a benchmark with ground truth. For each group, we show an example pair, and the statistics of all 45 pairs. The histograms comprise geodesic distances between found matches and the ground truth.

which contains 10 isometrically deformed shapes. Every pair of shapes in a group offers a test case, resulting in 90 cases in total count. In Fig. 10, we show an example pair and the statistics of 45 pairs for each group. The histograms comprise geodesic distances between found matches and the ground truth. Specifically, for each registered point on the reference shape, we compute the geodesic distance between its found match and the ground-truth point on the target shape, using the average edge length as the unit. The evaluation demonstrates that our method perform registration with high accuracy on complete shapes.

Quantitative method for evaluating experiments on real scans. The real scans have distortions and natural deformations, which are a challenge we must tackle in this paper. For quantitative evaluation, we calculate the histogram of edge length differences of registered shapes. The edge length difference refers to the absolute difference of an edge length in the reference shape and the corresponding length (which may not be an edge) in the target shape, using the average edge length as the unit for the normalization purpose. For isometric deformations and natural deformations (e.g., facial

expression, articulated movement), the edge length difference is expected to be very close to zero. Since we locate correspondence on the existed points, the resolution of our registration method is approximately 1, and the expected edge length difference is in $[0, 1]$. However, the histogram of edge length difference alone might not faithfully reflect the accuracy of registration. An extreme case is that, all the points in the reference shape are registered to the same point in the target shape. In this case, the edge length differences are all close to 1. Therefore, we also color code the output correspondences to directly visualize the registration results. The two approaches collectively can better evaluate the registration results.

Face scans. Fig. 11 shows two examples of face scans. Our method finds about 10 feature matches with meaningful saliences. Registrations are propagated from the matched features to other points. In this experiment, we let $t = 80$, and the vicinity size is 2-ring. We stop the registration when the propagation approaches to the boundary, where the mismatch increases. From the histogram in Fig. 11, we observe that most of the edge lengths
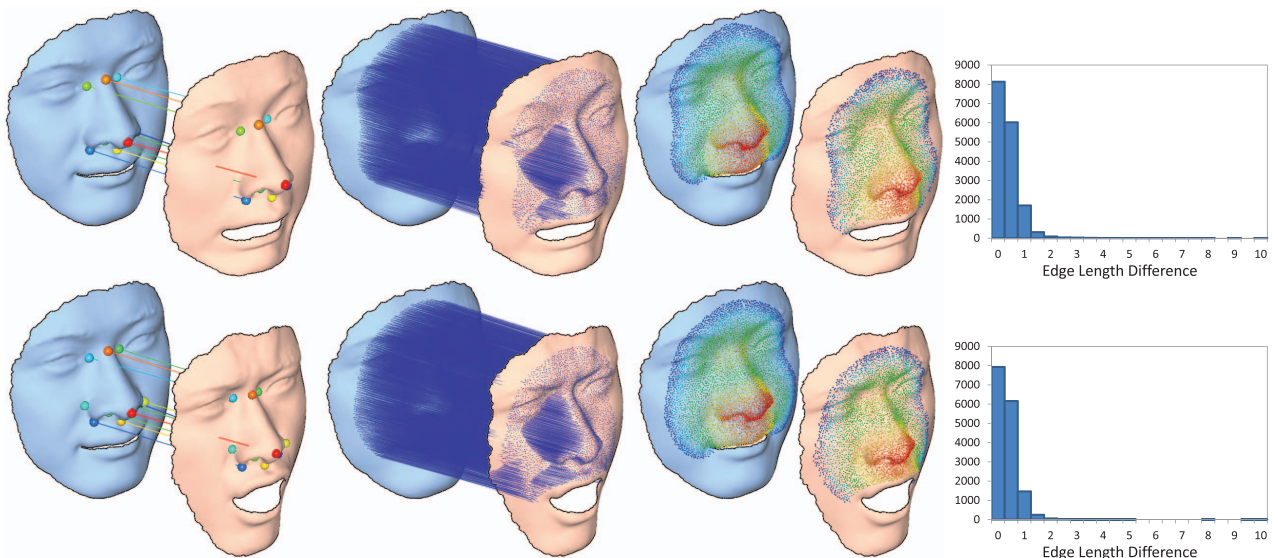
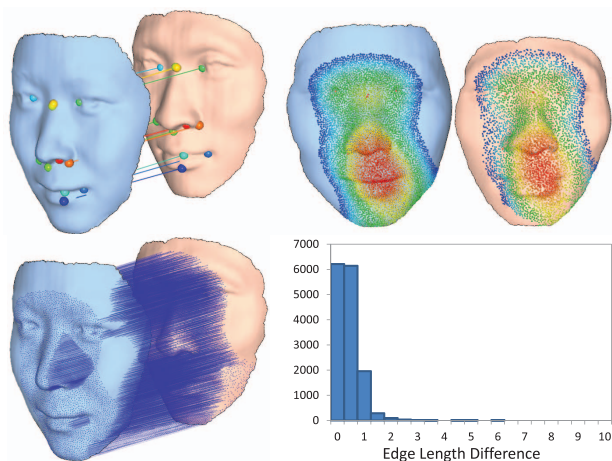

Fig. 11. Experiments on face scans.

Fig. 12. Experiment on similar but different shapes. A woman's face is registered to a man's face.

(a) Gaussian noise

(b) Small holes

(c) Large topology change

Fig. 13. Experiment on partial shapes under noise, small holes, and a large topology change.

fall into $[0, 1]$. The experimental result demonstrates that our method can find accurate correspondences on face scans, and is very stable under facial expressions.

Similar objects. Moreover, our method can handle some different yet similar objects. Fig. 12 shows an experimental result, where a woman's face is registered to a man's face. We accept more features in feature detection, aiming to create more candidates for feature matching. We reset the parameter $\sigma_2 = 1$ in (15) to increase the affinities of feature pairs, which weighs more on geometric compatibility than feature similarity. This experiment demonstrates that our method has great tolerance on distortion and noise, with a potential to be used for expression or motion transfer. It shows that the nature of our method relies more on the probability and geometric compatibility, not on single-point similarity.

Robustness. This experiment in Fig. 13 is to examine the robustness of our method under some challenging cases. We add Gaussian noise (with standard deviation $\sigma = 80\%$ of average edge length) to perturb vertex coordinates along their normals (first row), punch small holes (topological noise) on the shapes (second row), and fill the big hole of the mouth on the reference shape to make a large topology change (third row). As shown by the results, our method is robust to local changes such as noise and small holes. Large topology changes severely affect the connecting paths between points, and hence the heat kernels. However, the influence is restricted to the area of the change (i.e., the mouth), since our method is locality driven. Points outside the mouth area are still well registered.

Articulated objects. Other than facial expression, another commonly seen natural deformation is the articulated movement. Articulated objects usually have long and thin branches, which are more challenging than face scans due to the complicated geometry. Figs. 14 and 15 show two results of partial shapes from a man and a woman. We use 3-ring as the vicinity size to increase the search area, and set time $t = 50$. The feature detection and matching in our method perform the same way as other examples shown earlier. In the dense registration, our method performs well in the areas of head and body. However, the ambiguity of positioning in long branches (e.g., arms) makes the registration very challenging, since we only have sources at branch ends. We notice that, thin branches (marked by
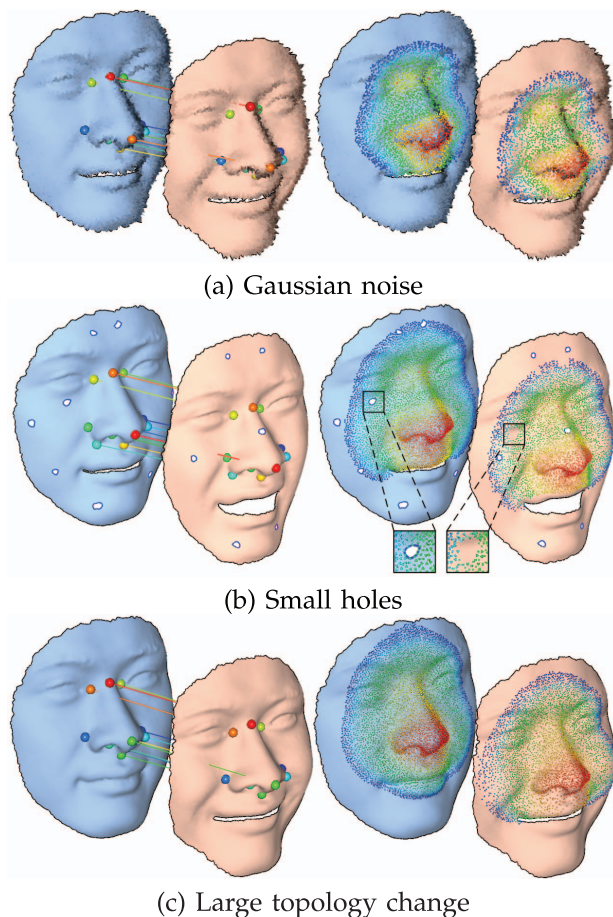
red circles) are more difficult than thick ones. Although it is extremely challenging, our method still outputs reasonable results quantitatively evaluated by the histograms of edge length differences.

Comparisons. Considering the similarity between the HKM and our method, we conduct this experiment to compare them on complete and partial shapes. For fairness, we use multiple sources for the HKM, which are found by our feature matching. Hence, the two methods have the same source points. We also apply the same parameters for the two methods. Fig. 16 shows a comparison on complete shapes. Since our method finds more feature matches as sources, both of the two methods lead to nice registration results. However, the HKM still has some flips at certain areas (e.g., the claws). The comparison in Fig. 17 is carried out on partial shapes with fewer sources available. On face scans, the HKM has some mismatches around the mouth. On articulated objects, large flips and mismatches start to appear in the HKM's result. The experimental results demonstrate that our searching algorithm improves the registration in propagating correspondences and avoiding large flips.

Time performance. We implement our method using C++ on a laptop with Core2 Duo CPU 2.53GHz and 4GB RAM. The time performance of selected experiments is shown in Table 1. Please note that, we did not list the time of computing the Laplace-Beltrami eigenfunctions. For all the experiments, we compute 300 eigenfunctions, which
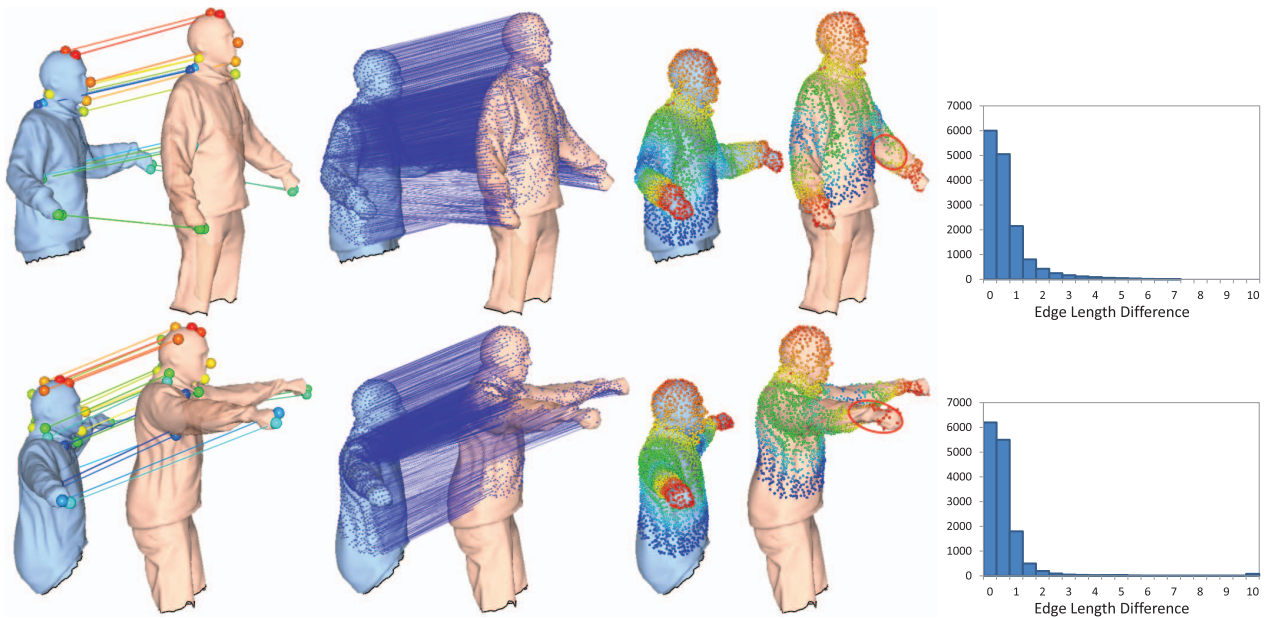
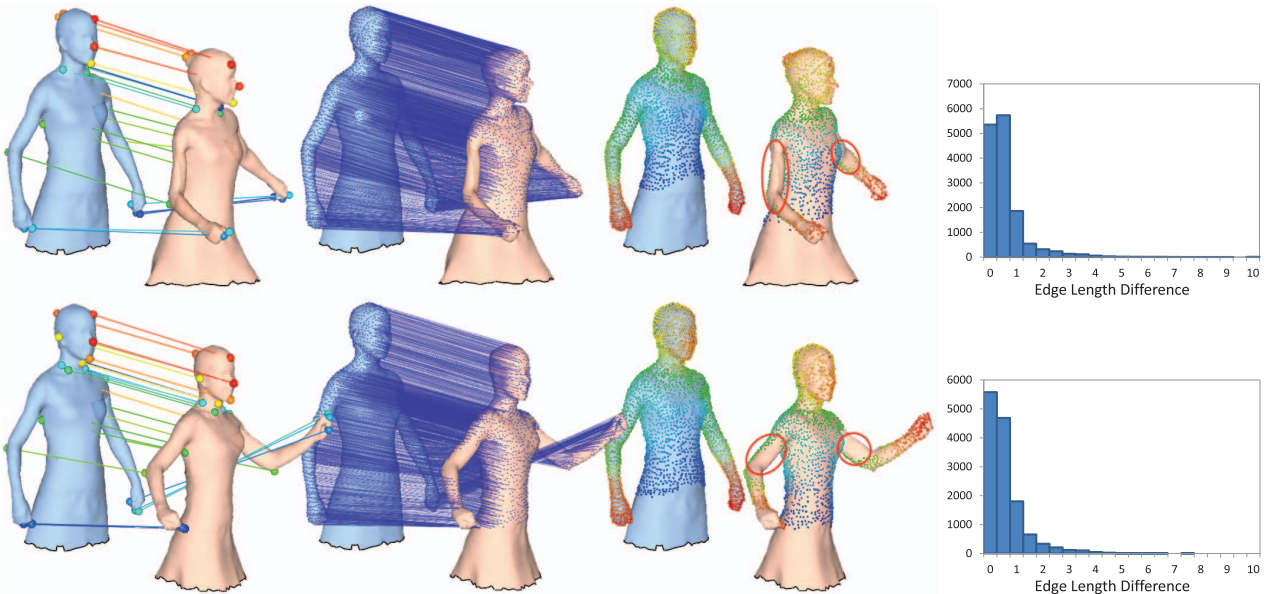Fig. 14. Experiment on articulated objects (man).

Fig. 15. Experiment on articulated objects (woman).

takes about 10 to 30 seconds for one shape, and can be accelerated by a multiresolution approach introduced in [25]. With computed Laplace-Beltrami eigenfunctions, our method is very efficient to complete feature detection, feature matching, and dense registration.

7 DISCUSSION

Based on the theoretical analysis and experimental results documented in previous sections, we address some limitations and open questions of our method as follows:

- Because of the diffusion nature of the HKCs, the uncertainty gradually increases when the heat diffusion approaches to boundaries from sources. As a result, the registration close to the boundary tends to be less trustworthy. Therefore, we may need

to ignore regions near the boundaries (as far as dense registration is concerned), though we can still proceed the registration if necessary.

- Although our method is robust to small holes, a large topology change may greatly affect heat kernels, and hence HKCs in the area of the change. To overcome this difficulty, one can repair the incorrect connections based on a template model or topology learning.

- As shown in the experiment of articulated objects, the registration in thin branches is not as good as near-flat regions due to the lack of features. We foresee that it can be solved if we have more features in those regions in a straightforward fashion.

- Generally speaking, more sources will produce more accurate correspondences. However, any mismatch in the initial feature matching can cause
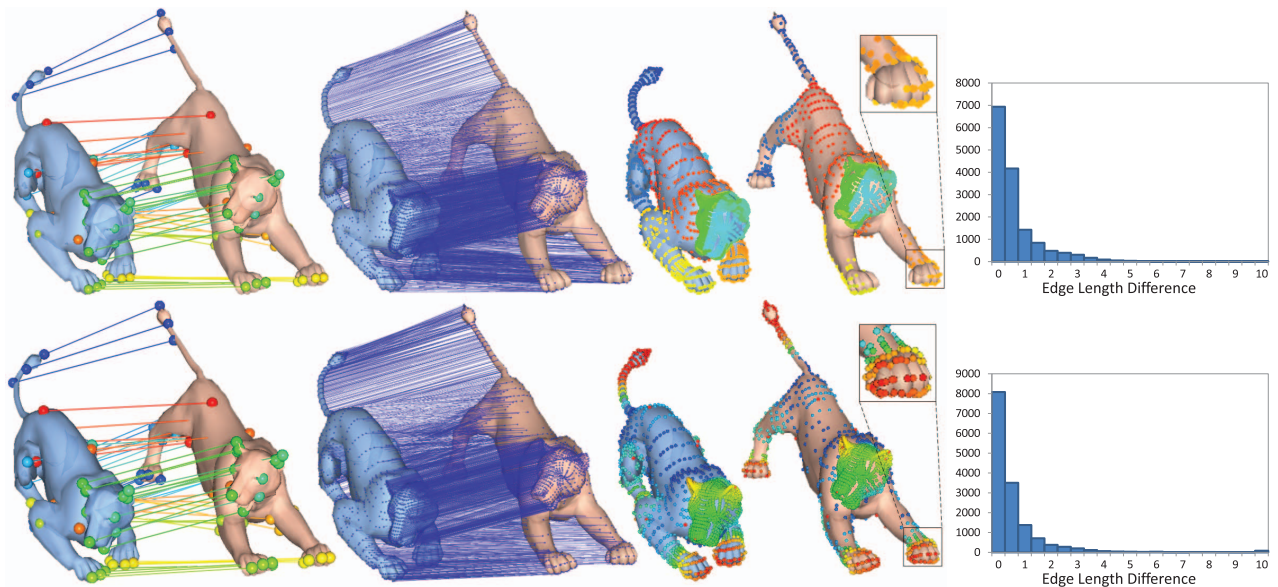
Fig. 16. Comparison with the multipoint HKM (first row) and our method (second row) on complete shapes. The two methods use the same source points found by our feature matching.
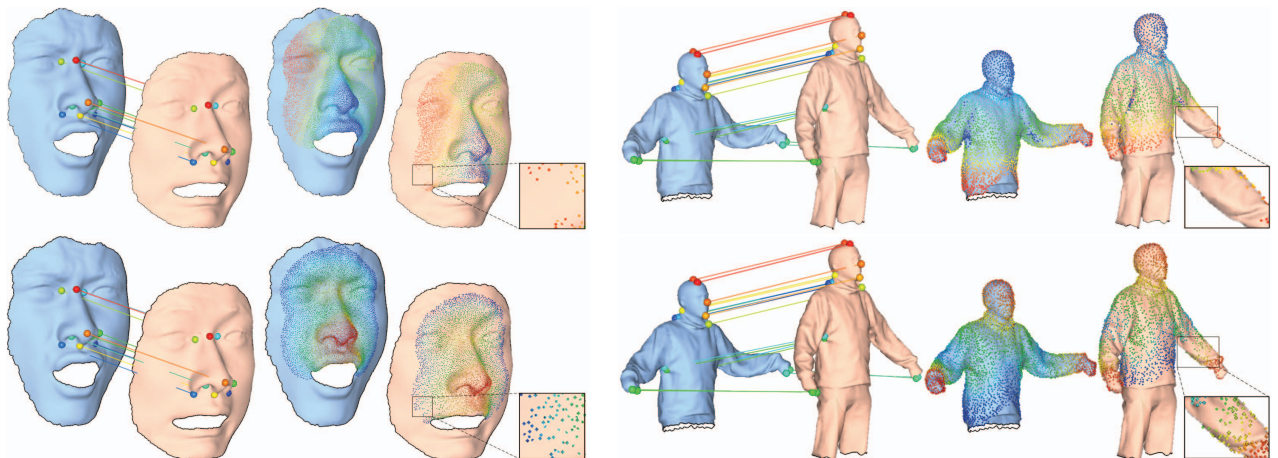

Fig. 17. Comparison with the multipoint HKM (first row) and our method (second row) on partial shapes. The two methods use the same source points found by our feature matching.

serious problems in registration. We use the robust HKS and graph matching to find stable feature matches, which have robustness yet sometimes find a few matches.

- Natural objects are usually symmetric. The ambiguity of symmetry can cause mismatches in feature matching. Although the graph matching considers geometric compatibility, it still remains a challenge if the shape is highly symmetric.

- Another outstanding issue is the parameter t for HKCs. While the value of t affects the HKCs and their priorities, we found that $t \in [20, 100]$ leads to results with similar qualities. In our experiments, we give the suggested value of t for every type of data sets as a feasible advice, yet the theoretic guarantee on time selection demands further investigation in the near future.

8   CONCLUSION

We have detailed a robust and complete method to address dense registration of partial nonrigid shapes. The challenge we are tackling in this paper shall serve as an impetus for a new research direction of space-time modeling of partial dynamic scans. The intrinsic HKCs can position and index points on the shape accurately. In our method, we offer novel and comprehensive solutions that aim to improve both

TABLE 1
Time Performance of Our Method in Seconds

Data	#V_1, #V_2	Computation Time		
		Feature	Match	Register
Cat (Fig. 10)	7.2k, 7.2k	0.75	1.86	16.38
Face (Fig. 11)	9.8k, 10.5k	1.39	0.19	4.70
Face (Fig. 12)	8.6k, 8.4k	2.21	1.51	4.68
Man (Fig. 14)	7.4k, 5.7k	1.34	1.24	6.66
Woman (Fig. 15)	6.1k, 6.2k	1.51	0.98	7.78
Lion (Fig. 16)	5.0k, 5.0k	0.50	2.24	12.84
Face (Fig. 17)	7.2k, 7.3k	1.98	0.58	2.95

efficiency and robustness in many aspects, including the time range of heat kernels, scaling scheme of the HKS, spectral matching with adaptive multiscale measurement, and priority-vicinity search. Our method affords dense registrations that are both feature driven and feature aligned. Upon extensive experiments on comprehensive data sets, we have demonstrated the performance of our method through visualized correspondences and quantitative evaluations.

For our ongoing efforts, we will work on possible improvements of our method, and continue the research along the direction of space-time modeling. Upon dense correspondences, we are capable of aligning the data in the space-time domain. It now sets a stage to employ piecewise continuous functions to model object geometry and its dynamic behavior in 4D toward model completion.

ACKNOWLEDGMENTS

REFERENCES

[1] V. Jain and H. Zhang, "Robust 3D Shape Correspondence in the Spectral Domain," *Proc. IEEE Int'l Conf. Shape Modeling and Applications (SMI)*, p. 19, 2006.

[2] Q.-X. Huang, B. Adams, M. Wicke, and L.J. Guibas, "Non-Rigid Registration under Isometric Deformations," *Computer Graphics Forum*, vol. 27, no. 5, pp. 1449-1457, 2008.

[3] Y. Lipman and T. Funkhouser, "Möbius Voting for Surface Correspondence," *ACM Trans. Graphics*, vol. 28, no. 3, pp. 72:1-72:12, 2009.

[4] O.K.-C. Au, C.-L. Tai, D. Cohen-Or, Y. Zheng, and H. Fu, "Electors Voting for Fast Automatic Shape Correspondence," *Computer Graphics Forum*, vol. 29, no. 2, pp. 645-654, 2010.

[5] T.K. Dey, K. Li, C. Luo, P. Ranjan, I. Safa, and Y. Wang, "Persistent Heat Signature for Pose-Oblivious Matching of Incomplete Models," *Computer Graphics Forum*, vol. 29, no. 5, pp. 1545-1554, 2010.

[6] M. Ovsjanikov, Q. Mérigot, F. Mémoli, and L. Guibas, "One Point Isometric Matching with the Heat Kernel," *Computer Graphics Forum*, vol. 29, no. 5, pp. 1555-1564, 2010.

[7] M.R. Ruggeri, G. Patanè, M. Spagnuolo, and D. Saupe, "Spectral-Driven Isometry-Invariant Matching of 3D Shapes," *Int'l J. Computer Vision*, vol. 89, nos. 2/3, pp. 248-265, 2010.

[8] J. Sun, X. Chen, and T.A. Funkhouser, "Fuzzy Geodesics and Consistent Sparse Correspondences for Deformable Shapes," *Computer Graphics Forum*, vol. 29, no. 5, pp. 1535-1544, 2010.

[9] O. van Kaick, H. Zhang, G. Hamarneh, and D. Cohen-Or, "A Survey on Shape Correspondence," *Proc. Eurographics State-of-The-Art Report*, pp. 1-24, 2010.

[10] M. Reuter, F.-E. Wolter, and N. Peinecke, "Laplace-Beltrami Spectra as "Shape-Dna" of Surfaces and Solids," *Computer-Aided Design*, vol. 38, no. 4, pp. 342-366, 2006.

[11] R.M. Rustamov, "Laplace-Beltrami Eigenfunctions for Deformation Invariant Shape Representation," *Proc. Fifth Eurographics Symp. Geometry Processing (SGP '07)*, pp. 225-233, 2007.

[12] T. Ju, S. Schaefer, and J. Warren, "Mean Value Coordinates for Closed Triangular Meshes," *ACM Trans. Graphics*, vol. 24, no. 3, pp. 561-566, 2005.

[13] P. Joshi, M. Meyer, T. De Rose, B. Green, and T. Sanocki, "Harmonic Coordinates for Character Articulation," *ACM Trans. Graphics*, vol. 26, no. 3, pp. 71:1-71:9, 2007.

[14] P.W. Jones, M. Maggioni, and R. Schul, "Manifold Parameterizations by Eigenfunctions of the Laplacian and Heat Kernels," *Proc. Nat'l Academy of Sciences of USA*, vol. 105, no. 6, pp. 1803-1808, 2008.

[15] T. Hou and H. Qin, "Efficient Computation of Scale-Space Features for Deformable Shape Correspondences," *Proc. 11th European Conf. Computer Vision (ECCV)*, pp. 384-397, 2010.

[16] Y. Zeng, C. Wang, Y. Wang, X. Gu, D. Samaras, and N. Paragios, "Dense Non-Rigid Surface Registration Using High-Order Graph Matching," *Proc. IEEE Conf. Computer Vision and Pattern Recognition (CVPR)*, pp. 382-389, 2010.

[17] J. Sun, M. Ovsjanikov, and L. Guibas, "A Concise and Provably Informative Multi-Scale Signature Based on Heat Diffusion," *Computer Graphics Forum*, vol. 28, no. 5, pp. 1383-1392, 2009.

[18] M. Leordeanu and M. Hebert, "A Spectral Technique for Correspondence Problems Using Pairwise Constraints," *Proc. IEEE 10th Int'l Conf. Computer Vision (ICCV)*, pp. 1482-1489, 2005.

[19] X. Gu, S. Wang, J. Kim, Y. Zeng, Y. Wang, H. Qin, and D. Samaras, "Ricci Flow for 3D Shape Analysis," *Proc. IEEE 11th Int'l Conf. Computer Vision (ICCV)*, 2007.

[20] J. Novatnack and K. Nishino, "Scale-Dependent 3D Geometric Features," *Proc. IEEE 11th Int'l Conf. Computer Vision (ICCV)*, pp. 1-8, 2007.

[21] C.H. Lee, A. Varshney, and D.W. Jacobs, "Mesh Saliency," *ACM Trans. Graphics*, vol. 24, no. 3, pp. 659-666, 2005.

[22] R. Gal and D. Cohen-Or, "Salient Geometric Features for Partial Shape Matching and Similarity," *ACM Trans. Graphics*, vol. 25, no. 1, pp. 130-150, 2006.

[23] J. Hua, Z. Lai, M. Dong, X. Gu, and H. Qin, "Geodesic Distance-Weighted Shape Vector Image Diffusion," *IEEE Trans. Visualization and Computer Graphics*, vol. 14, no. 6, pp. 1643-1650, Nov./Dec. 2008.

[24] G. Zou, J. Hua, Z. Lai, X. Gu, and M. Dong, "Intrinsic Geometric Scale Space by Shape Diffusion," *IEEE Trans. Visualization and Computer Graphics*, vol. 15, no. 6, pp. 1193-1200, Nov./Dec. 2009.

[25] A. Vaxman, M. Ben-Chen, and C. Gotsman, "A Multi-Resolution Approach to Heat Kernels on Discrete Surfaces," *ACM Trans. Graphics*, vol. 29, no. 4, pp. 121:1-121:10, 2010.

[26] G. Patanè and B. Falcidieno, "Multi-Scale Feature Spaces for Shape Processing and Analysis," *Proc. Shape Modeling Int'l Conf. (SMI '10)*, pp. 113-123, 2010.

[27] A. Dubrovina and R. Kimmel, "Matching Shapes by Eigendecomposition of the Laplace-Beltrami Operator," *Proc. 3D Data Processing, Visualization and Transmission*, 2010.

[28] A.M. Bronstein, M.M. Bronstein, M. Mahmoudi, R. Kimmel, and G. Sapiro, "A Gromov-Hausdorff Framework with Diffusion Geometry for Topological-Robust Non-Rigid Shape Matching," *Int'l J. Computer Vision*, vol. 89, nos. 2/3, pp. 266-286, 2010.

[29] M.M. Bronstein and A.M. Bronstein, "Shape Recognition with Spectral Distances," *IEEE Trans. Pattern Analysis and Machine Intelligence*, vol. 33, no. 5, pp. 1065-1071, May 2011.

[30] D. Raviv, A.M. Bronstein, M.M. Bronstein, R. Kimmel, and N. Sochen, "Affine-Invariant Diffusion Geometry for the Analysis of Deformable 3D Shapes," *Computers & Graphics*, vol. 35, no. 3, pp. 692-697, 2011.

[31] T. Cour, P. Srinivasan, and J. Shi, "Balanced Graph Matching," *Proc. Conf. Neural Information Processing Systems*, pp. 313-320, 2006.

[32] L. Torresani, V. Kolmogorov, and C. Rother, "Feature Correspondence via Graph Matching," *Proc. 10th European Conf. Computer Vision*, pp. 596-609, 2008.

[33] O. Duchenne, F. Bach, I. Kweon, and J. Ponce, "A Tensor-Based Algorithm for High-Order Graph Matching," *Proc. IEEE Conf. Computer Vision and Pattern Recognition*, pp. 1980-1987, 2009.

[34] W. Chang and M. Zwicker, "Automatic Registration for Articulated Shapes," *Computer Graphics Forum*, vol. 27, no. 5, pp. 1459-1468, 2008.

[35] V. Kraevoy and A. Sheffer, "Cross-Parameterization and Compatible Remeshing of 3D Models," *ACM Trans. Graphics*, vol. 23, no. 3, pp. 861-869, 2004.

[36] V. Jain, H. Zhang, and O. van Kaick, "Non-Rigid Spectral Correspondence of Triangle Meshes," *Int'l J. Computer Vision*, vol. 13, no. 1, pp. 101-124, 2007.

[37] D. Mateus, R. Horaud, D. Knossow, F. Cuzzolin, and E. Boyer, "Articulated Shape Matching Using Laplacian Eigenfunctions and Unsupervised Point Registration," *Proc. IEEE Conf. Computer Vision and Pattern Recognition (CVPR)*, pp. 1-8, 2008.

[38] M. Reuter, F.-E. Wolter, M. Shenton, and M. Niethammer, "Laplace-Beltrami Eigenvalues and Topological Features of Eigenfunctions for Statistical Shape Analysis," *Computer-Aided Design*, vol. 41, no. 10, pp. 739-755, 2009.

[39] N. Ahmed, C. Theobalt, C. Rössl, S. Thrun, and H.-P. Seidel, "Dense Correspondence Finding for Parametrization-Free Animation Reconstruction from Video," *Proc. IEEE Conf. Computer Vision and Pattern Recognition (CVPR)*, pp. 1-8, 2008.

[40] A.M. Bronstein, M.M. Bronstein, and R. Kimmel, "Generalized Multidimensional Scaling: A Framework for Isometry-Invariant Partial Surface Matching," *Proc. Nat'l Academy of Sciences of USA,* vol. 103, no. 5, pp. 1168-1172, 2006.

[41] A. Tevs, M. Bokeloh, and M. Wand, "Isometric Registration of Ambiguous and Partial Data," *Proc. IEEE Conf. Computer Vision and Pattern Recognition (CVPR),* pp. 1185-1192, 2009.

[42] A. Grigor'yan, "Heat Kernels on Weighted Manifolds and Applications," *Contemporary Math.,* vol. 398, pp. 93-191, 2006.

[43] R. Liu and H. Zhang, "Mesh Segmentation via Spectral Embedding and Contour Analysis," *Computer Graphics Forum,* vol. 26, no. 3, pp. 385-394, 2007.

[44] F. de Goes, S. Goldenstein, and L. Velho, "A Hierarchical Segmentation of Articulated Bodies," *Computer Graphics Forum,* vol. 27, no. 5, pp. 1349-1356, 2008.

[45] M. Reuter, "Hierarchical Shape Segmentation and Registration via Topological Features of Laplace-Beltrami Eigenfunctions," *Int'l J. Computer Vision,* vol. 89, no. 2, pp. 287-308, 2010.

[46] M. Meyer, M. Desbrun, P. Schröder, and A.H. Barr, "Discrete Differential-Geometry Operators for Triangulated 2-Manifolds," *Visualization and Math.,* vol. 3, no. 7, pp. 35-57, 2002.

[47] A. Grigor'yan and L. Saloff-Coste, "Heat Kernel on Manifolds with Ends," *Annales de l'institut Fourier,* vol. 59, no. 5, pp. 1917-1997, 2009.

[48] L. Saloff-Coste, "The Heat Kernel and its Estimates," *Advanced Studies in Pure Math.,* vol. 57, 2010.

[49] R.R. Coifman, S. Lafon, A.B. Lee, M. Maggioni, B. Nadler, F. Warner, and S.W. Zucker, "Geometric Diffusions as a Tool Fro Harmonic Analysis and Structure Definition of Data: Diffusion Maps," *Proc. Nat'l Academy of Sciences of USA,* vol. 102, no. 21, pp. 7426-7431, 2005.

[50] A. Grigor'yan, "Escape Rate of Brownian Motion on Riemannian Manifolds," *Applicable Analysis,* vol. 71, no. 1, pp. 63-89, 1999.

[51] R.W. Sumner and J. Popović, "Deformation Transfer for Triangle Meshes," *ACM Trans. Graphics,* vol. 23, no. 3, pp. 399-405, 2004.

[52] L. Zhang, N. Snavely, B. Curless, and S. Seitz, "Spacetime Faces: High-Resolution Capture for Modeling and Animation," *ACM Trans. Graphics,* vol. 23, no. 3, pp. 548-558, 2004.

[53] S. Wang, X. Gu, and H. Qin, "Automatic Non-Rigid Registration of 3D Dynamic Data for Facial Expression Synthesis and Transfer," *Proc. IEEE Conf. Computer Vision and Pattern Recognition (CVPR),* pp. 1-8, 2008.

[54] D. Vlasic, I. Baran, W. Matusik, and J. Popović, "Articulated Mesh Animation from Multi-View Silhouettes," *ACM Trans. Graphics,* vol. 27, no. 3, pp. 97:1-97:9, 2008.

Tingbo Hou received the BS degree from University of Science and Technology of China in 2004, and the M.E. degree from Chinese Academy of Sciences in 2007. Currently, he is working toward the PhD degree in Department of Computer Science at Stony Brook University (SUNY at Stony Brook), USA. His research interests include visual computing, shape analysis, shape matching/registration, surface reconstruction, data completion, geometric modeling, and computational photography. He is a student member of the IEEE.

Hong Qin received the BS degree and the MS degrees in computer science from Peking University, China. He received the PhD degree in computer science from the University of Toronto. Currently, he is a professor of computer science in Department of Computer Science at State University of New York at Stony Brook (Stony Brook University). During his years at the University of Toronto (UofT), he received UofT Open Doctoral Fellowship. He was also a recipient of NSF CAREER Award from the National Science Foundation (NSF), Honda Initiation Award, and Alfred P. Sloan Research Fellow by the Sloan Foundation. Currently, he serves as an associate editor for The Visual Computer, Graphical Models, and Journal of Computer Science and Technology. His research interests include geometric and solid modeling, graphics, physics-based modeling and simulation, computer aided geometric design, human-computer interaction, visualization, and scientific computing. He is a senior member of the IEEE. Detailed information about him can be found from his website: http://www.cs.sunysb.edu/qin.

▷ **For more information on this or any other computing topic, please visit our Digital Library at** www.computer.org/publications/dlib.